Structural analysis and crystal-field calculations of Nd^{3+} in $Gd_xLu_{1-x}TaO_4$ ($x = 0.85$) polycrystalline*

Gao Jin-Yun(高进云)[a)b)], Zhang Qing-Li(张庆礼)[a)†], Yang Hua-Jun(杨华军)[a)b)], Zhou Peng-Yu(周鹏宇)[a)b)], Sun Dun-Lu(孙敦陆)[a)], Yin Shao-Tang(殷绍唐)[a)], and He Ye(何 晔)[c)]

[a)] *Anhui Provincial Key Laboratory of Photonic Devices and Materials, Anhui Institute of Optics and Fine Mechanics, Chinese Academy of Sciences, Hefei* 230031, *China*

[b)] *Graduate School of the Chinese Academy of Sciences, Beijing* 100049, *China*

[c)] *China Electronics Technology Group Corporation, No. 26 Research Institute, Chongqing* 400060, *China*

(Received 17 February 2012; revised manuscript received 4 May 2012)

The crystal structural parameters of Nd^{3+}-doped rare earth orthotantalate $Gd_xLu_{1-x}TaO_4$ ($x = 0.85$) are determined by applying the Rietveld refinement to its X-ray diffraction, and its emission and excitation spectra at 77 K are analysed. The relativistic model of *ab initio* self-consistent DV-Xα method, which is applied to the cluster NdO_8 in $Gd_xLu_{1-x}TaO_4$, and the effective Hamiltonian model are used to investigate its spin–orbit and crystal-field parameters. The free-ions and crystal-field parameters are fitted to the experimental energy levels at 77 K with a root-mean-square deviation of 14.92 cm^{-1}. According to the crystal-field calculations, 96 levels of Nd^{3+} are assigned. Finally, the fitting results of free-ions and crystal-field parameters are compared with those already reported for Nd^{3+}:$YAlO_3$. The results indicate that the free-ion parameters are similar to those of the Nd^{3+} in $Gd_xLu_{1-x}TaO_4$ and $YAlO_3$ hosts, and the crystal-field interaction of Nd^{3+} in $Gd_xLu_{1-x}TaO_4$ is stronger than that in $YAlO_3$.

Keywords: rare earth orthotantalate, crystal structure, optical properties, DV-Xα method, crystal-field calculations

PACS: 61.66.–f, 31.15.A–, 71.70.Ch, 75.10.Dg **DOI:** 10.1088/1674-1056/21/10/106103

1. Introduction

High density inorganic scintillators are very important in many fields such as high energy physics and medical imaging. Although some heavy scintillators such as $PbWO_4$, BGO, Ce:LSO, and Ce:LuAP with density values of 8.28, 7.13, 7.35, and 6.69 g/cm^3, respectively, are used in practice, scintillators with higher density and better performance are still desired.[1−3] The density of monoclinic RETaO$_4$ (RE = La to Lu) is in a range of 8.8 g/cm^3–9.8 g/cm^3, and is far higher than those of the above-mentioned scintillators.[4,5] It has been reported[6,7] that the structures of rare-earth orthotantalates RETaO$_4$ (RE = La to Lu) have two crystallographic structures: one is high-temperature phase with space group $B2/b$, which is named M-type, and the other is low-temperature phase with space group $P2/a$ and named M′-type. Both of the structures could be considered as a monoclinic distortion of the scheelite structure and their main difference lies in the coordination of Ta atom. In an M-type structure, the Ta atoms are assembled as a tetrahedron, while in M′-type, the Ta atoms exist in a distorted octahedron. Luminescence properties of rare-earth tantalates have been reported by Blasse and Brill.[8] Paramagnetic anisotropies in crystal RETaO$_4$ (RE = Nd, Ho, and Er) have been reported by Tsunekawa *et al.*[9] Photoluminescence properties of RE^{3+}:LuTaO$_4$ (RE = Eu, Tb) with an M′-type structure has been reported by Wen-Peng Liu *et al.*[5] Among these rare-earth tantalates, M-type GdTaO$_4$ and LuTaO$_4$ have been proved to be promising hosts for efficient luminescent materials.[8,10] Nd-doped, Yb-doped, and Er-doped GdTaO$_4$ single crystals are grown successfully with Czochralski method by our group, but it is very difficult to grow the single crystal LuTaO$_4$, of which its density is the highest of the rare-earth orthotantalates. Furthermore, if Gd in GdTaO$_4$ is replaced by Lu partially, its density will be higher. On the other hand, the site symmetry of Nd^{3+} is C_2 and very low, which is advantageous for relaxing

*Project supported by the National Natural Science Foundation of China (Grant Nos. 90922003, 51172236, and 50872135) and the Knowledge Innovation Program of the Chinese Academy of Sciences (Grant No. YYYJ-1002).

†Corresponding author. E-mail: zql@aiofm.ac.cn

© 2012 Chinese Physical Society and IOP Publishing Ltd

the parity-forbidden rule and improving its photoluminescence efficiency. So, 1 at% Nd^{3+}:$Gd_xLu_{1-x}TaO_4$ ($x = 0.85$) with a density of 9.07 g/cm^3 polycrystalline is synthesized, and its spectral property and crystal-field are also studied in order to evaluate its application future in this work.

There are generally two methods to study the spectral properties and energy level structures of the $4f^N$ configuration of rare-earth ions doped in crystal. First of all, the crystal-field model has been widely and successfully applied to the parameterization of the energy levels of the 4f configuration in various crystal hosts. The crystal-field fitting calculations and energy level structures of Nd^{3+} in various hosts have been reported in particular.[11−15] On the other hand, the *ab initio* calculations are primarily based on Hartree–Fork theory and its perturbation theory, and they have been used for many decades.[16−19] Because a heavy rare-earth element whose inner orbit has many electrons and their relativistic effect is very strong, and it is a system of N 4f electrons in different environments of hosts, the results from *ab initio* calculations are not consistent with the experimental results. Therefore, *ab initio* calculations and crystal-field fitting calculations were combined to study the crystal field of Nd^{3+}:$Gd_xLu_{1-x}TaO_4$ in this work.

To start with, determined in this work are the structures of $Gd_xLu_{1-x}TaO_4$ and Nd^{3+}:$Gd_xLu_{1-x}TaO_4$ ($x = 0.85$) by using the Rietveld method, thereby obtaining the structural data for further *ab initio* calculations. Then, the spin–orbit and crystal-field parameters of Nd^{3+} in $Gd_xLu_{1-x}TaO_4$ ($x = 0.85$) are calculated from the effective Hamiltonian model reported previously by Reid *et al.*[20] In this model, eigenvalues and eigenvectors from DV-Xα calculation are used to construct the effective Hamiltonian. Finally, these parameters are also used as the initial parameters to fit the experimental levels obtained from the emission and excitation spectra. So far, no relevant reports about the energy level fitting and crystal-field calculations of Nd^{3+} in $Gd_xLu_{1-x}TaO_4$ ($x = 0.85$) have been found to our knowledge.

2. Models

2.1. DV-Xα method

The self-consistent DV-Xα method is less computer-time-consuming than other *ab initio* calculation methods, and thus suited to treat large molecules and sizable clusters representing solid-state systems. Heavy atoms such as transition-metals, lanthanides, and actinides, may also be included.[21] The essential points of its relativistic molecular calculation are shown in the following for our proposal.[22]

The time-independent Dirac equation of a single electron can be written as

$$\left(c\boldsymbol{\alpha}\cdot\boldsymbol{p}+mc^2\boldsymbol{\beta}+V(\boldsymbol{r})-\varepsilon_i\right)\varphi_i(\boldsymbol{r},\zeta)=0, \quad (1)$$

where $\boldsymbol{p} = -\mathrm{i}\hbar\nabla$ is the momentum operator, m is the mass of the single electron, ε_i is the electronic energy of the single electron, c=137.037 is the velocity of light in atomic unit (a.u.), $V(\boldsymbol{r})$ is an approximation to the potential seen by an electron with (space, spin) 4-vector coordinates $(\boldsymbol{r},\zeta)$, and $\boldsymbol{\alpha}$ and $\boldsymbol{\beta}$ are the velocity operators and given as

$$\boldsymbol{\alpha}=\begin{pmatrix}0 & \boldsymbol{\sigma}\\ \boldsymbol{\sigma} & 0\end{pmatrix} \quad \text{and} \quad \boldsymbol{\beta}=\begin{pmatrix}\boldsymbol{I} & 0\\ 0 & -\boldsymbol{I}\end{pmatrix}, \quad (2)$$

where $\boldsymbol{\sigma}$ represents the 2×2 Pauli matrix and $\boldsymbol{I}$ is the 2×2 unit matrix.

In the Dirac–Slater model of DV-Xα method, the molecular one-electron functions $\varphi_i(\boldsymbol{r},\zeta)$ are expanded as a linear combination of numerical atomic-like orbital $\chi_j(\boldsymbol{r},\zeta)$

$$\varphi_i(\boldsymbol{r},\zeta)=\sum_j c_i^j\chi_j(\boldsymbol{r},\zeta), \quad (3)$$

where c_i^j is the coefficient of $\chi_j(\boldsymbol{r},\zeta)$. Taking the atomic-like orbital χ_j as the basis vectors and then solving the Dirac equation leads to the four-dimensional matrix equation

$$(\boldsymbol{H}-\varepsilon\boldsymbol{S})\boldsymbol{C}=0, \quad (4)$$

where $\boldsymbol{H}$ is the matrix of the the Dirac Hamiltonian, $\boldsymbol{S}$ is the matrix of the overlap integral between the basis vector, and $\boldsymbol{C}$ is the matrix coefficient. So, we carry out the self-consistently iterative calculations repeatedly until the convergent precision is less than 10^{-3}.

In the $Gd_xLu_{1-x}TaO_4$ (x= 0.85) polycrytalline, Nd^{3+} ions mainly replace the sites of Gd^{3+} and Lu^{3+} surrounded by eight nearest-neighbour oxygen ions. So we adopt the cluster NdO_8. In fact, we think that the large cluster calculation results are unreasonable in the sense of physical significance, indicated by analysing the proportion of the atomic orbital. Especially in large clusters, the higher state in the Gd (Lu) atomic orbital may be mixed with the composition of the conduction band, which can be confirmed

from the experimental line-width data and the optical conductivity.[23] The initial structural parameters of $Gd_xLu_{1-x}TaO_4$ ($x = 0.85$) are obtained from the results of the Rietveld refinement to X-ray diffraction. In the actual calculation process, some internal orbits are frozen, and basis sets are selected as the numerical atomic basis (NAO). The parameters of the basis sets and the potential well are shown in Table 1.

Table 1. Parameters of basis sets and potential well.

Ions	Frozen core	Orbit of basis functions	Parameters of Funnel potential well/a.u.		
			V_0	R_1	R_2
Nd^{3+}	1s–4d	4f, 5s, 5p, 5d, 6s	–2.0	2.0	3.3
O^{2-}	1s	2s, 2p	–2.0	4.0	6.0

The sampling point distribution has selected Diophantus rules. The number of network points of each atomic symmetry analysis is 90; the standard effectively taken as zero is 10^{-6}; the standard of degeneration is 1.000001; the iterated precision of self-consistency is 10^{-4}; the exchange parameter is 0.66667, the number of blocks of integral points is 50; the frequency of self-consistency is 200.[24,25]

2.2. Crystal-field fitting calculations

The complex energy level scheme of the Nd^{3+} ion in the crystal results from the interactions—both within the $4f^3$ electron configuration and between the Nd^{3+} ion and its environment. A parametric model Hamiltonian used in this study can be written as

$$\hat{H} = \hat{H}_{\rm A} + \hat{H}_{\rm CF}, \tag{5}$$

where $\hat{H}_{\rm A}$ denotes the atomic Hamiltonian and $\hat{H}_{\rm CF}$ the crystal-field interaction Hamiltonian. The $\hat{H}_{\rm A}$ operator can be written as

$$\begin{aligned}\hat{H}_{\rm A} = {} & E_{\rm avg} + \sum_{k=2,4,6} F^k \hat{f}_k + \xi \hat{A}_{\rm SO} + \alpha \hat{L}(\hat{L}+1) \\ & + \beta \hat{G}(G_2) + \gamma \hat{G}(R_7) \\ & + \sum_{i=2,3,4,6,7,8} T^i \hat{t}_i + \sum_{j=0,2,4} M^j \hat{m}_j \\ & + \sum_{k=2,4,6} P^k \hat{p}_k. \end{aligned} \tag{6}$$

In this expression, parameter $E_{\rm avg}$ is the spherically symmetric one-electron part of the Hamiltonian; the electrostatic interaction is described with the Slater integrals $F^k f_k$ ($k = 2$, 4, and 6), where F^k and f_k are the radial part and the angular part, respectively; ξ and $A_{\rm SO}$ are the radial part and the angular part of spin–orbit interaction, respectively; α, β, and γ are two-body electrostatic parameters, G (G_2) and G (R_7) are Casimir operators for the G_2 and R_7 groups, and L is the total orbital angular-momentum; $T^i t_i$ ($i = 2$, 3, 4, 6, 7, and 8) describe the three-body configuration interactions, where T^i is a parameter and t_i is an operator; higher-order magnetic spin–spin and spin–other-orbit interactions as well as the electrostatically correlated spin–orbit interactions can be represented by Marvin integrals M^j ($j = 0$, 2, and 4) and P^k ($k = 2$, 4, and 6), and the operators associated with these parameters are designated by m_j and p_k, respectively. The parameters obey the ratios $M^2 = 0.56M^0$, $M^4 = 0.38M^0$, and $P^4 = 0.75P^2$, $P^6 = 0.5P^2$.[26,27]

The $\hat{H}_{\rm CF}$ can be expressed as

$$\begin{aligned}\hat{H}_{\rm CF} = {} & \sum_{k,q} B_q^k C_q^{(k)} \\ & (k = 2, 4, 6, \quad \text{and} \quad q = -k \le q \le k), \end{aligned} \tag{7}$$

where B_q^k are the crystal-field parameters and $C_q^{(k)}$ is an angular part spherical tensor operator.[28] For the C_2 symmetry of Nd^{3+} doped in $Gd_xLu_{1-x}TaO_4$ ($x = 0.85$) polycrytalline, it has the following non-vanished crystal-field parameters: B_0^2, B_2^2, B_0^4, B_2^4, B_4^4, B_0^6, B_2^6, B_4^6, B_6^6, where B_0^2, B_2^2, B_0^4, B_0^6 are real and B_2^4, B_4^4, B_2^6, B_4^6, B_6^6 are complex. Thus, the crystal-field Hamiltonian is expressed as follows:

$$\begin{aligned}\hat{H}_{\rm CF}(C_2) = {} & \sum_k B_0^k C_0^k + \sum_{k,q>0} [{\rm Re}B_q^k \left(C_q^k + C_{-q}^k\right) \\ & + {\rm i}{\rm Im}B_q^k \left(C_q^k - C_{-q}^k\right)] \end{aligned} \tag{8}$$

with $k = 2$, 4, 6, and $q \le k$.[29]

The crystal-field parameters are fitted by the calculations of a set of crystal-field parameters from experimentally determined crystal-field split energy levels. An iterative least-square fitting procedure is generally required as follows:[30]

(i) estimate initial values of the crystal-field parameters for the system under consideration or *ab initio* calculations;

(ii) construct the energy matrix using estimated or previously calculated crystal-field parameters;

(iii) diagonalize the energy matrix to obtain its eigenvalues, which correspond to estimated positions of the energy levels;

(iv) set up one-to-one correspondences between the experimental and calculated energy levels;

(v) keep the eigenvectors of the energy matrix unchanged, determine the values of the parameters that minimize the sum of squares of the differences between the calculated and experimental energy levels;

(vi) substitute the set of crystal-field parameter values derived from step (v) back into step (ii) and continue iterating steps (ii)–(v) until the calculated and experimental energy levels are judged to be in good enough agreement.

The parameter set is optimized in a general least-squares fitting by minimizing the squares of the differences between the experimental and calculated energy levels. The root-mean-square deviation (σ) is used as a figure of merit to describe the quality of the fit, and it is given as[31]

$$\sigma = \left(\frac{\sum \left(E_{\rm exp} - E_{\rm calc} \right)^2}{N - P} \right)^{1/2}, \tag{9}$$

where $E_{\rm exp}$ and $E_{\rm calc}$ are the experimental and calculated energy levels, respectively, N is the number of experimental energy levels, and P is the number of variable parameters. The σ is to be reduced to a value as small as possible. If σ is less than 20 $\rm cm^{-1}$, it is believed that the parameter set can give a good description of the system.

Once the crystal-field parameters are obtained, we can estimate the crystal-field strength N_ν as defined by Auzel and Malta[32] for the garnet structure hosts as follows:

$$N_v = \left(\sum_{k,q} \frac{4\pi}{2k+1} \left| B_q^k \right|^2 \right)^{1/2}, \tag{10}$$

where the values of N_ν are calculated from the two sets of crystal-field parameters, which are defined in terms of the length rather than the rotational invariants of the crystal-field parameter vector in the spherical harmonics space, allowing a direct comparison of the crystal-field strength in any type of symmetry.

3. Results and discussion

3.1. Experimental and structural determination

The $Gd_xLu_{1-x}TaO_4$ and 1 at% Nd^{3+}:$Gd_xLu_{1-x}TaO_4$ ($x = 0.85$) were synthesized by using the high temperature solid-state reaction method. The starting materials were Gd_2O_3, Lu_2O_3, Ta_2O_5, and Nd_2O_3 with a purity of 99.99%. The materials were thoroughly mixed and calcined at 1500 °C for 48 h and then naturally cooled to room temperature in the furnace. The phase-transition temperature was about 1480 °C, and after cooling we obtained the M-type structure $Gd_xLu_{1-x}TaO_4$ and 1 at% Nd^{3+}:$Gd_xLu_{1-x}TaO_4$ ($x = 0.85$) with space group $B2/b$. Due to the fact that the radius ratio between ions Nd^{3+} and Gd^{3+} is close to that between ions Nd^{3+} and Lu^{3+}, the Nd^{3+} ions of the host occupy the sites of Gd^{3+} ions rather than those of Lu^{3+} ions.

The powder X-ray diffraction (XRD) was carried out by using a Philips X'pert PRO diffractometer with Cu Kα radiation at room temperature in step-scanned mode in a range from 10° to 90° with step-scan interval of 0.03°. The structures of $Gd_xLu_{1-x}TaO_4$ ($x = 0.85$) and 1 at% Nd^{3+}:$Gd_xLu_{1-x}TaO_4$ ($x = 0.85$) were refined by using the general structure analysis system (GSAS)[33] according to their XRD. Using the structural data of $GdTaO_4$ (the inorganic crystal structure database (ICSD), card No. 153362) as initial values, we refined 32 parameters including profile parameters, atom coordinates, temperature, background curve parameters, and so on. The refined results of $Gd_xLu_{1-x}TaO_4$ ($x = 0.85$) and 1 at% Nd^{3+}:$Gd_xLu_{1-x}TaO_4$ ($x = 0.85$) polycrytalline material are shown in Figs. 1 and 2, respectively.

In Figs. 1 and 2, the observed, calculated, and their difference curves of the refinement to their XRD patterns are shown. The residuals $R_{\rm p}$ and $R_{\rm wp}$ of $Gd_xLu_{1-x}TaO_4$ ($x = 0.85$) are 5.49%, 7.64%, and Nd^{3+}:$Gd_xLu_{1-x}TaO_4$ ($x = 0.85$) are 6.47% and 8.15%, which are very small, indicating that the observed and calculated XRD patterns are consistent very well. The fitted structural parameters by Rietveld refinement are listed in Table 2.

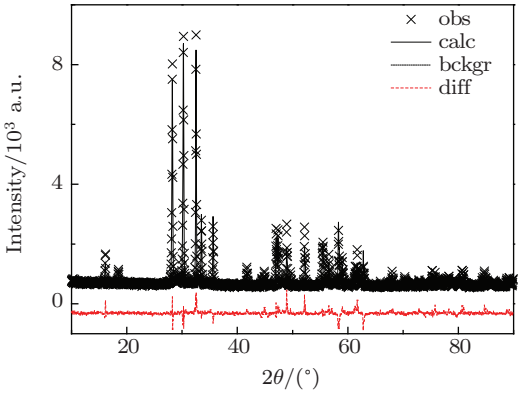


Fig. 1. X-ray powder diffraction patterns and Rietveld fitting curve of $Gd_xLu_{1-x}TaO_4$ ($x = 0.85$) polycrystalline material.

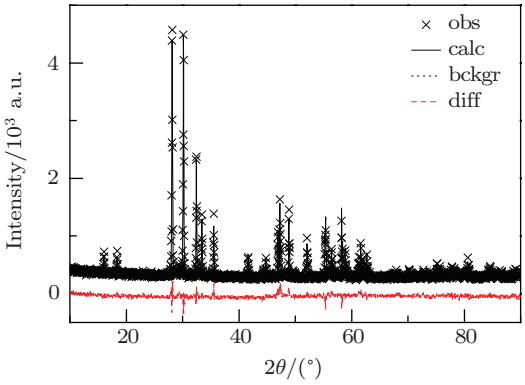


Fig. 2. X-ray powder diffraction patterns and Rietveld fitting curve of Nd^{3+}:$Gd_xLu_{1-x}TaO_4$ ($x = 0.85$) polycrystalline material.

Table 2. Structural parameters of $Gd_xLu_{1-x}TaO_4$ ($x = 0.85$) and Nd^{3+}:$Gd_xLu_{1-x}TaO_4$ ($x = 0.85$), which are obtained by Rietveld refinement to their X-ray powder diffraction, 1 Å=0.1 nm.

Material		$Gd_xLu_{1-x}TaO_4$ ($x = 0.85$)		Nd^{3+}:$Gd_xLu_{1-x}TaO_4$ ($x = 0.85$)	
atom	site	x, y, z	U_{iso}/Å^2	x, y, z	U_{iso}/Å^2
Nd, Gd and Lu*	4e1	0, 0.25, 0.6288	0.0011	0, 0.25, 0.6315	0.0211
Ta	4e2	0, 0.25, 0.1023	0.0208	0, 0.25, 0.1011	0.0138
O1	8f1	0.201, 0.139, 0.134	0.0857	0.174, 0.127, 0.182	0.0630
O2	8f2	0.258, 0.290, 0.402	0.0645	0.240, 0.276, 0.441	0.0411
Lattice		a=7.030, b=5.076, c=11.031		a=7.030, b=5.075, c=11.029	
Parameters		γ=130.35°, V=299.89		γ=130.35°, V=299.89	
R factor		R_p = 5.49%, R_{wp} = 7.64%		R_p = 6.47%, R_{wp} = 8.15%	

*Gd, Lu, and Nd ions occupy the 4e1 site, so constraint on isotropic atomic displacement factor of $U_{iso}(Nd) = U_{iso}(Gd) = U_{iso}(Lu)$ is used.

3.2. Spectral analysis

The complete $4f^3$ configuration of Nd^{3+} ions consists of 364 Stark energy levels, which are 182 Kramers' doubly degenerate levels, and the transitions between all Stark levels are allowed as both electric and magnetic dipole transitions.[34]

The emission spectrum (λ_{ex} = 808 nm) and excitation spectrum (λ_{em} = 1068 nm) of 1 at% Nd^{3+}:$Gd_xLu_{1-x}TaO_4$ ($x = 0.85$) are shown in Figs. 3 and 4, respectively. The emission and excitation spectrum are both measured at 77 K, which is more accurate than those measured at room temperature. The characteristic emission bands under 808-nm excitation (shown as Fig. 3) are ascribed to the transitions from $^4F_{3/2}$ to ^4I_J (J = 9/2, 11/2, and 13/2) of Nd^{3+}, of which the emission peak at 1068 nm of $^4F_{3/2} \rightarrow {}^4I_{11/2}$ transition is the strongest. Therefore, the excitation spectrum is measured with a monitor wavelength 1068 nm, which is shown in Fig. 4, and the 14 spectral bands correspond to transitions of $^4I_{9/2} \rightarrow {}^2H(1)_{11/2} + {}^2D(2)_{5/2}$, $^2I_{13/2} + {}^2L_{17/2} + {}^4D_{7/2}\ldots$, $^2I_{11/2} + {}^2L_{15/2} + {}^4D_{5/2} + {}^4D_{3/2}\ldots$, $^2P_{3/2} + {}^4D_{5/2}$, $^2P_{1/2}$, $^2G(1)_{9/2} + {}^4G_{11/2} + {}^2D(1)_{3/2} + {}^2K_{15/2}$, $^2K_{13/2} + {}^4G_{9/2}$, $^4G_{7/2}$, $^4G_{5/2} + {}^2G_{7/2}$, $^2H(2)_{11/2}$, $^4F_{9/2}$, $^4S_{3/2} + {}^4F_{7/2}$, $^4F_{5/2} + {}^2H(2)_{9/2}$, and $^4F_{3/2}$ of Nd^{3+}, respectively.

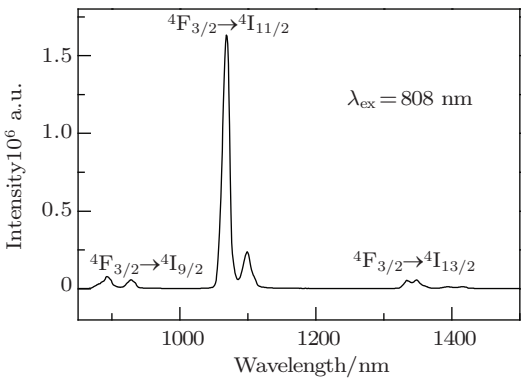


Fig. 3. Emission spectrum of 1 at% Nd^{3+}:$Gd_xLu_{1-x}TaO_4$ ($x = 0.85$) (λ_{ex} = 808 nm).

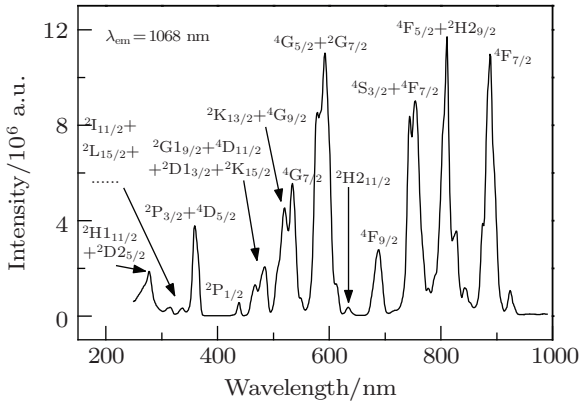


Fig. 4. Excitation spectrum of 1 at% Nd^{3+}:$Gd_xLu_{1-x}TaO_4$ ($x = 0.85$) ($\lambda_{em} = 1068$ nm).

Based on the above consideration, the absorption spectra allow us to discern 96 energy levels from among the 364 Stark energy levels of the $4f^3$ (Nd^{3+}) configuration.

3.3. Calculations of energy levels

Using the relativistic model of *ab initio* self-consistent DV-Xα method[21,22] and effective Hamiltonian model,[20] the crystal-field and spin–orbit parameters of Nd^{3+} in $Gd_xLu_{1-x}TaO_4$ ($x = 0.85$) are calculated. The parameters of Nd^{3+} in $Gd_xLu_{1-x}TaO_4$ ($x = 0.85$) are shown in Table 3.

Table 3. Parameters of Nd^{3+} in $Gd_xLu_{1-x}TaO_4$ ($x = 0.85$).

Parameters	Nd^{3+}:$Gd_xLu_{1-x}TaO_4$ ($x = 0.85$)
B_0^2	–1554
B_2^2	–462
B_0^4	–312
B_2^4	1072+49i
B_4^4	–219+466i
B_0^6	–656
B_2^6	278-139i
B_4^6	922+28i
B_6^6	10+156i
ξ	946

The experimental energy level values of Nd^{3+} are obtained from the previous spectroscopic analysis. Then, the crystal-field and spin–orbit parameters from DV-Xα method and effective Hamiltonian method and other free-ion parameters from Ref. [35] are used as the initial values to fit the experimental energy levels of Nd^{3+} in $Gd_xLu_{1-x}TaO_4$ ($x = 0.85$) with the f-shell fitting program, which is developed by Ried[12,13] in Fortran language. The calculated results, experiment results, and their difference are shown in Table 4.

Table 4. Energy levels of Nd^{3+} in $Gd_xLu_{1-x}TaO_4$ ($x = 0.85$).

$^{2S+1}L_J$	Energy levels			$^{2S+1}L_J$	Energy levels		
	E (calc)	E (exp)	$\Delta E/cm^{-1}$		E (calc)	E exp	$\Delta E/cm^{-1}$
$^4I_{9/2}$	14.05	0	–14.05	$^4G_{7/2}$	17946.32	17927	–19.32
	105.78	102	–3.78		18029.23	–	–
	203.68	218	14.32		19526.40	–	–
$^4I_{11/2}$	327.38	337	9.62		19667.14	19653	–14.14
	571.08	598	26.92		19736.87	–	–
	2263.84	2269	5.16		19873.37	19873	-0.37
	2348.81	2351	2.19		19994.19	–	–
	2426.31	–	–		20072.94	–	–
	2479.48	2482	2.52		20159.86	–	–
	2563.97	2558	–5.97		20232.50	–	–
	2702.25	2721	18.75	$^2K_{13/2}$ + $^4G_{9/2}$	20330.94	–	–
	4550.74	4548	–2.74		20439.79	–	–
	4624.54	4632	7.46		20477.60	–	–
$^4I_{13/2}$	4710.15	–	–		20506.19	20512	5.81
	4739.04	4735	–4.04		20536.19	–	–
	4824.73	4818	–6.73		20556.06	–	–
	4926.91	4920	–6.91		20615.95	–	–
	5067.46	–	–		20882.44	–	–

Table 4. (*Continued*).

$^{2S+1}L_J$	Energy levels			$^{2S+1}L_J$	Energy levels		
	E (calc)	E (exp)	ΔE/cm^{-1}		E (calc)	E exp	ΔE/cm^{-1}
	6829.38	–	–		21664.99	21670	5.01
	6878.10	–	–		21752.88	–	–
	7032.68	–	–		21865.30	–	–
$^4I_{15/2}$	7056.82	–	–		21979.21	–	–
	7136.63	–	–		22051.05	–	–
	7290.25	–	–		22152.44	22149	–3.44
	7443.23	–	–		22262.72	–	–
	7589.70	–	–		22350.00	–	–
$^4F_{3/2}$	11599.66	11604	4.34	$^2G_{9/2}(1) + {}^4G_{11/2} + {}^2D_{3/2}(1) + {}^2K_{15/2}$	22407.17	–	–
	11865.41	11844	–21.41		22447.67	–	–
	12746.25	12737	–9.25		22511.41	–	–
	12821.24	12824	2.76		22579.87	–	–
$^4F_{5/2} + {}^2H_{9/2}(2)$	12895.27	12877	–18.27		22647.88	–	–
	12936.65	12925	–11.65		22669.46	–	–
	13043.89	13048	4.11		22721.24	–	–
	13059.94	–	–		22810.27	–	–
	13122.43	–	–		22847.28	22841	–6.28
	13187.75	13164	–23.75		22930.47		
	13896.60	13911	14.40		22957.33		
	14074.48	14072	–2.48		23007.17		
$^4F_{7/2} + {}^4S_{3/2}$	14109.14	–	–		23213.66		
	14139.85	14164	24.15	$^2P_{1/2}$	23943.68	23924	–19.68
	14202.62	–	–		24466.69	–	–
	14339.26	–	–	$^2D_{5/2}(1)$	24792.25	–	–
	15411.58	15421	9.42		25029.22	–	–
	15513.31	15532	18.69		27334.82	–	–
$^4F_{9/2}$	15656.80	15654	–2.80	$^2P_{3/2}$	27582.08	27612	29.92
	15742.72	–	–		28346.75	–	–
	15774.45	15763	–11.45		28638.00	–	–
	16784.02	16799	14.98	$^4D_{3/2}\ {}^4D_{5/2}\ {}^2I_{11/2}\ {}^4D_{1/2} \ldots$	...	–	–
	16798.85	–	–		29651.98	29621	–30.98
$^2H_{11/2}(2)$	16857.69	–	–		...	–	–
	16860.88	–	–		31049.42	–	–
	16874.97	16882	7.03	$^2I_{13/2}\ {}^2L_{17/2}\ {}^4D_{7/2} \ldots$	...	–	–
	16905.58	16910	4.42		31661.65	31676	14.35
	17502.76	–	–		...	–	–
	17577.34	17568	–9.34		35197.21	–	–
$^4G_{5/2} + {}^2G_{7/2}$	17699.26	–	–	$^2D_{5/2}(2)\ {}^2H_{11/2}(1) \ldots$	...	–	–
	17868.95	17884	15.05		35743.52	35716	–27.52
	17902.70	–	–		...	–	–

From Table 4, most of the calculated levels coincide with the experimental energy levels very well. Among the 96 experimental energy levels at 77 K, there are seven Stark levels (598, 11844, 13164, 14164, 27612, 29621, and 35716 cm^{-1}) with poor fitting quality with deviations of 26.92, −21.41, −23.75, 24.15, 29.92, −30.98, and −27.52 cm^{-1}, respectively. The deviation of calculated energy levels and experimental energy levels are less than 32 cm^{-1}, which indicates that the theoretical results are satisfactory.

It is concluded that the J-mixing effect does not play any significant role in the low-lying energy levels from fitting results, especially for $^4I_{9/2}$, $^4I_{11/2}$, $^4I_{13/2}$, $^4I_{15/2}$, and $^4F_{3/2}$ multiplets. However, at the higher-

energy side, the J-mixing effect is clearly appreciable because the Stark components overlap with adjacent multiplets. On the other hand, the M-mixing effect is very clear for all energy levels. For example, the wavefunction component ratios corresponding to $E = 0$ and 12824 cm^{-1} of Nd^{3+} are as follows:

$$\begin{aligned}
E &= 0\ \text{cm}^{-1},\\
\psi_1 &= 67\% \times (0.37 + 0.73\text{i}) \times \left|{}^4\text{I}_{9/2,1/2}\right\rangle\\
&\quad + 24\% \times (-0.28 - 0.40\text{i}) \times \left|{}^4\text{I}_{9/2,-3/2}\right\rangle,\\
\psi_2 &= 67\% \times (-0.77 + 0.28\text{i}) \times \left|{}^4\text{I}_{9/2,-1/2}\right\rangle\\
&\quad + 24\% \times (0.48 - 0.11\text{i}) \times \left|{}^4\text{I}_{9/2,3/2}\right\rangle;\\
E &= 12824\ \text{cm}^{-1},\\
\psi_3 &= 31\% \times (0.34 - 0.44\text{i}) \times \left|{}^2\text{H}\,(2)_{9/2,5/2}\right\rangle\\
&\quad + 26\% \times (0.23 - 0.45\text{i}) \times \left|{}^4\text{F}_{5/2,5/2}\right\rangle,\\
\psi_4 &= 31\% \times (0.14 - 0.54\text{i}) \times \left|{}^2\text{H}\,(2)_{9/2,-5/2}\right\rangle\\
&\quad + 26\% \times (0.22 - 0.46\text{i}) \times \left|{}^4\text{F}_{5/2,-5/2}\right\rangle.
\end{aligned}$$

3.4. Crystal-field analysis

The experimental energy levels of Nd^{3+} give a basic set for a reliable energy level simulation. A model with 30 parameters including 16 free-ion and 14 crystal-field parameters is used for Nd^{3+} in $Gd_xLu_{1-x}TaO_4$ ($x = 0.85$), with a root-mean-square deviation (σ) of 14.92 cm^{-1}. In the simulation process, it can be stated that the relative positions of some experimental energy levels depend on α, β, γ, and T^i. For example the energy levels of $^4S_{3/2}$ and $^4F_{7/2}$, $^4G_{9/2}$, and $^2K_{13/2}$, $^4G_{11/2}$, and $^2K_{15/2}$.[36]

The free-ion and crystal-field parameters of Nd^{3+} in $Gd_xLu_{1-x}TaO_4$ ($x = 0.85$) and $YAlO_3$ hosts are shown in Table 5. The parameters of Nd^{3+} in $YAlO_3$ are cited from Ref. [37].

The values of free-ion parameters of Nd^{3+} in $Gd_xLu_{1-x}TaO_4$ ($x = 0.85$) are similar to those in $YAlO_3$ hosts. However, the electrostatic interaction between two 4f electrons of Nd^{3+}:$Gd_xLu_{1-x}TaO_4$ ($x = 0.85$) is stronger than that of Nd^{3+}:$YAlO_3$, because of the more delocalized electrons and decreased Slater integrals. With the Slater integrals decreasing, the individual $^{2S+1}L_J$ state will be lowered, so the energy positions of $^2P_{1/2}$ are 23924 cm^{-1} and 23164 cm^{-1} for Nd^{3+} in $Gd_xLu_{1-x}TaO_4$ ($x = 0.85$) and $YAlO_3$ hosts, respectively. The spin–orbit interaction varies slightly for these two hosts whereas the other free-ion parameters show no clear trend. This is because the Nd^{3+} ion occupies the 4e site of Gd (Lu) with C_2 point symmetry, and each of the ions in $Gd_xLu_{1-x}TaO_4$ ($x = 0.85$) is octahedrally coordinated with six O ions, forming a distorted square antiprism. Whereas the Nd^{3+} ion occupies the 4c site of Y with C_S point symmetry, and each of the ions is dodecahedrally coordinated to eight O ions in $YAlO_3$.

Table 5. Comparisons between Nd^{3+}:$Gd_xLu_{1-x}TaO_4$ ($x = 0.85$) and Nd^{3+}:$YAlO_3$ in terms of free-ion and crystal-field parameters.

Parameters	Nd^{3+}:$Gd_xLu_{1-x}TaO_4$ ($x = 0.85$)	Nd^{3+}:$YAlO_3$[a]
E_{avg}	25136(17)	24119(3)
F^2	73018(65)	70925(25)
F^4	52789(87)	50794(67)
F^6	35757(39)	35424(63)
ξ	917 (3)	875(2)
α	21(1.2)	23(0.2)
β	–593(13)	–691(8)
γ	1445(32)	[1690]
T^2	298(17)	458(9)
T^3	35(2)	38(3)
T^4	59(4)	75(5)
T^6	–285(30)	–290(10)
T^7	332(81)	237(11)
T^8	305(142)	496(28)
M	2.11(0.23)	1.90(0.20)
P	192(24)	206(39)
B_0^2	–1551(29)	–154(47)
B_2^2	–476(52)	578(18)
B_0^4	–475(55)	–541(79)
B_2^4	1305+46i(54+51i)	967+24i(39+74i)
B_4^4	–307+451i(60+43i)	–309+608i(62+62i)
B_0^6	–581(76)	–671(97)
B_2^6	235–136i(81+103i)	512–18i(65+145i)
B_4^6	808+28i(49+17i)	1611+[0i](35)
B_6^6	–99+158i(83+96i)	0+132i(52+107i)
σ	14.92	15.50
N_ν	3284	2545

[a] The free-ion and crystal-field parameters of Nd^{3+}:$YAlO_3$ cited from Ref. [37].

The values of crystal-field parameters are affected by the distances, bonding angles, and the nature of ligands.[28] The crystal-field parameters B^4 and B^6 are related only to the ions of the nearest neighbour rather than the ions of next nearest neighbour and further, while B^2 ions are related not only to the ions of the nearest neighbour but also to the ions of next nearest neighbour and further. In Table 5, crystal-field parameters B_0^2 and B_2^2 of Nd^{3+}:$Gd_xLu_{1-x}TaO_4$ ($x = 0.85$) and Nd^{3+}:$YAlO_3$ have relatively large dif-

ferences, but other crystal-field parameters are close to each other. This is because the interaction between 4f electrons of Nd^{3+} and Ta^{5+}, Gd^{3+}, and Lu^{3+} surrounding Nd^{3+} are strong in $Gd_xLu_{1-x}TaO_4$ ($x = 0.85$). It is indicated that the charge interpenetration and Coulomb exchange of Nd^{3+}:$Gd_xLu_{1-x}TaO_4$ ($x = 0.85$) are stronger than those of Nd^{3+}:$YAlO_3$ while covalency and overlap of Nd^{3+}:$Gd_xLu_{1-x}TaO_4$ ($x = 0.85$) are weaker than those of Nd^{3+}:$YAlO_3$. In fact, the overlap and Coulomb exchange are responsible for about half the total parameters values, the other half mostly originate from covalency. When the charge penetration contributions are taken into account, the magnitudes of the net electrostatic contributions are only on the order of 10% of the combined contributions from covalency and exclusion. So in the analysis of the lanthanide crystal fields, approximation in which the electrostatic contributions are neglected, is likely to be far more realistic than that in which overlap and covalency are ignored.[38]

The values of N_ν are calculated from the two sets of crystal-field parameters, which are defined in terms of the length rather than the rotational invariants of the crystal-field parameters vector in the spherical harmonics space, allowing a direct comparison with the crystal-field strength in any type of symmetry.[29] From Table 5, we see that the contribution of rank six crystal-field parameters to the total crystal-field strength is larger in $Gd_xLu_{1-x}TaO_4$ ($x = 0.85$) than that in $YAlO_3$. Taking into consideration the electronegativity values of Gd (Lu) and Y ions, it might be concluded that in $Gd_xLu_{1-x}TaO_4$ ($x = 0.85$) crystals, the neighbour ions of impurities are slightly nearer than those in the $YAlO_3$ crystals, so that the contribution to the total crystal field of these neighbours is greater in $Gd_xLu_{1-x}TaO_4$ ($x = 0.85$) than that in the $YAlO_3$ hosts, as indicated from the calculations. Thus the N_ν of Nd^{3+} in $Gd_xLu_{1-x}TaO_4$ ($x = 0.85$) is larger than that in $YAlO_3$, therefore, the crystal-field interaction of $Gd_xLu_{1-x}TaO_4$ ($x = 0.85$) is stronger than that of $YAlO_3$.

4. Conclusion

The structure of Nd^{3+}:$Gd_xLu_{1-x}TaO_4$ ($x = 0.85$) with M-type is determined with X-ray diffraction, and its emission and excitation spectra in 77 K are analysed. The *ab initio* self-consistent DV-Xα method is used in its relativistic model to investigate the crystal-field and spin–orbit parameters of Nd^{3+}:$Gd_xLu_{1-x}TaO_4$ ($x = 0.85$). With the crystal-field and spin–orbit parameters from DV-Xα and effective Hamiltonian methods, the energy levels of Nd^{3+} in $Gd_xLu_{1-x}TaO_4$ ($x = 0.85$) are fitted. The 96 experimental energy levels of Nd^{3+} are assigned with a root-mean-square deviation (σ) of 14.92 cm^{-1}. It is found that the deviations of the calculated energy levels from experimental energy levels are less than 32 cm^{-1}, which indicates that the energy level fitting results are satisfactory. These results could be used to calculate the spectral parameters, absorption cross section and so on in the further work.

References

[1] Pontes F M, Maurera M A, Souza A G, Longo E, Leite E R, Magnani R, Machado M A C, Pizani P S and Varela J A 2003 *J. Eur. Ceram. Soc.* **23** 3001

[2] Gironnet J, Mikhailik V B, Kraus H, de Marcillac P and Coron N 2008 *Nucl. Instr. Method* A **594** 358

[3] Lempicki A, Glodo J and Coron N 1998 *Nucl. Instr. Method* A **416** 333

[4] Forbes T Z, Nyman M, Rodriguez M A and Navrotsky A 2010 *J. Solid State Chem.* **183** 2516

[5] Liu W P, Zhang Q L, Ding L H, Sun D L, Luo J Q and Yin S T 2009 *J. Alloys Compd.* **474** 226

[6] Cava R J, Murphy D W and Zahurak S M 1983 *J. Electrochem. Soc.* **130** 2345

[7] Silva R A, Tirao G, Cusatis C and Andreeta J P 2005 *J. Cryst. Growth* **274** 512

[8] Blasse G and Brill A 1970 *J. Lumin.* **3** 109

[9] Tsunekawa S, Yamauchi H, Sasaki K, Yamaguchi Y and Fukuda T 1996 *J. Alloys Compd.* **245** 89

[10] Li B, Gu Z N, Lin J H and Su M Z 2000 *J. Mater. Sci.* **35** 1139

[11] Rukmini E, Jayasankar C K and Reid M F 1994 *J. Phys.: Condens. Matter* **6** 5919

[12] Burdick G W, Jayasankar C K, Richardson F S and Reid M F 1994 *Phys. Rev.* B **50** 16309

[13] Rudowicz C, Chua M and Reid M F 2000 *Physica* B **291** 327

[14] Zhang Q L, Ning K J, Xiao J, Ding L H, Zhou W L, Liu W P, Yin S T and Jiang H H 2010 *Chin. Phys.* B **19** 087501

[15] Song T, Sun X W, Liu Z J, Li J F and Tian J H 2012 *Chin. Phys.* B **21** 037103

[16] Slater J C 1951 *Phys. Rev.* **81** 385

[17] Sun Y, Liu L, Dong J P, Zhang B and Huang X J 2011 *Chin. Phys.* B **20** 126101

[18] Li T X, Wang L, Wang F, Chen J, Jiang Z Y and Li L S 2011 *Chin. Phys.* B **20** 033101

[19] Li J, Liu X Y, Zhu Z H and Sheng Y 2012 *Chin. Phys.* B **21** 033101

[20] Reid M F, Duan C K and Zhou H W 2009 *J. Alloys Compd.* **488** 591

[21] Ellis D E and Painter G S 1970 *Phys. Rev.* B **2** 2887

[22] Rosen A and Ellis D E 1975 *J. Chem. Phys.* **62** 3039

[23] Pieterson L, Reid M F, Wegh R T, Soverna S and Meijerink A 2002 *Phys. Rev.* B **65** 045113
[24] Ning L X, Zhang L Y, Hu L S, Yang F, Duan C K and Zhang Y F 2011 *J. Phys.: Condens. Matter* **23** 205502
[25] Hu L S, Reid M F, Duan C K, Xia S D and Yin M 2011 *J. Phys.: Condens. Matter* **23** 045501
[26] Christiane G W and Koen B, in: Gschneidner K A and Eyring L (edt.), 1996 *Handbook on the Physics and Chemistry of Rare Earths* (Amsterdam, New York, Oxford: North-Holland Publishing Company) **23** pp. 143–152
[27] Karbowiak M, Edelstein N M, Drozdzynski J and Kossowski K 2002 *Chem. Phys.* **277** 362
[28] Xia S D 1994 *Group Theory and Spectroscopy* (Beijing: Science Press) pp. 262–283 (in Chinese)
[29] Loro H, Vasquez D, E Camarillo G, Castillo H Del, Munoz G, C Flores J, J Hernandez A and Murrieta S H 2007 *Phys. Rev.* B **75** 125405-8
[30] Newman D J and Betty N 2000 *Crystal Field Handbook* (Cambridge: Cambridge University Press) pp. 43–46
[31] Christiane G W and Koen B, in: Gschneidner K A and Eyring L (edt.), 1996 *Handbook on the Physics and Chemistry of Rare Earths* (Amsterdam, New York, Oxford: North-Holland Publishing Company) **23** p. 164
[32] Auzel F and Malta O L 1983 *J. Phys.* **44** 201
[33] Rietveld H M 1969 *J. Appl. Crystallogr.* **2** 65
[34] Antic-Fidancev E, Holsa J and Lastusaari M 2003 *J. Phys.: Condens. Matter* **15** 863
[35] Molina P, Loro H, Álvarez-García S, Bausá L E, Rodriguez E Martín, Guillot-Noël O, Goldner Ph, Bettinelli M, Ghigna P and Solé J García 2009 *Phys. Rev.* B **80** 054111-8
[36] da Gama A A S and de Gilberto F Sa 1981 *J. Chem. Phys.* **75** 2583
[37] Duan C K, Tanner P A, Makhov V N and Kirm M 2007 *Phys. Rev.* B **75** 195130
[38] Newman D J and Betty N 2000 *Crystal Field Handbook* (Cambridge: Cambridge University Press) pp. 24–26